Energy Conversion and Management 87 (2014) 367–377

Contents lists available at ScienceDirect

Energy Conversion and Management

journal homepage: www.elsevier.com/locate/enconman

Electro-thermal characterization of Lithium Iron Phosphate cell with equivalent circuit modeling

L.H. Saw *, Y. Ye, A.A.O. Tay

Department of Mechanical Engineering, Faculty of Engineering, National University of Singapore, Singapore 117576, Singapore

ARTICLE INFO

Article history:
Received 6 March 2014
Accepted 2 July 2014
Available online 31 July 2014

Keywords:
Battery temperature
Electric vehicles
Equivalent circuit modeling
Heat generation
Lithium Iron Phosphate battery

ABSTRACT

Prediction of the battery performance is important in the development of the electric vehicles battery pack. A battery model that is capable to reproduce *I–V* characteristic, thermal response and predicting the state of charge of the battery will benefit the development of cell and reduce time to market for electric vehicles. In this work, an equivalent circuit model coupled with the thermal model is used to analyze the electrical and thermal behavior of Lithium Iron Phosphate pouch cell under various operating conditions. The battery model is comprised three RC blocks, one series resistor and one voltage source. The parameters of the battery model are extracted from pulse discharge curve under different temperatures. The simulations results of the battery model under constant current discharge and pulse charge and discharge show a good agreement with experimental data. The validated battery model is then extended to investigate the dynamic behavior of the electric vehicle battery pack using UDDS and US06 test cycle. The simulation results show that an active thermal management system is required to prolong the calendar life and ensure safety of the battery pack.

1. Introduction

High capacity lithium-ion battery is an attractive choice for the automotive energy storage system in hybrid electric vehicles (HEVs) and electric vehicles (EVs) battery pack. The success of the EVs greatly depends on the development of the Li-ion battery. The battery used to power the vehicles is exposed to more severe operating conditions than portable electronic gadgets such as extreme operating temperature in the cold and hot environment (−40 °C to 70 °C), and high charge and discharge rate [1]. Besides, Li-ion batteries should operate within 25–40 °C for optimum performance and calendar life [2]. In addition, it is desirable to maintain the temperature variation between battery modules in the battery pack less than 5 °C [2]. Under high temperature, the capacity fading of the cell is more significant and the separator in the cell could melt, causing an internal short circuit and leading to uncontrollable temperature rise (thermal runaway) [3]. On the other hand, lithium plating will occur at temperature below 0 °C, charging and discharging of the cell become impossible. The lithium plating is permanent and cannot be removed with cycling of the cell [3]. Moreover, 10 years of calendar life targeted by the United States Advanced Battery Consortium further imply that significant efforts are needed in the development of the battery thermal management system for automotive applications [4].

Thermal response of the EV battery pack has been an interest to the researchers due to their potential thermal runaway and degradation of the performance under high temperature operating condition [5]. Laboratory and field test are commonly used to characterize the thermal response of the battery pack under the requirement of the transient power response [6–8]. Zolot et al. investigated the performance of the Toyota Prius battery pack under different driving cycle (HWFET, FTP and US06) at various environmental temperatures. The thermal performance of the battery pack at 25 °C is excellent for all the cycle [7]. However, experimental testing of the battery pack always required expensive facility such as high power programmable battery cycler and huge environment chamber to accommodate the battery pack. Moreover, experimental testing does not encourage innovative design and optimization of the battery pack [6]. Therefore, numerical simulation could be used to overcome the drawbacks in the experimental testing of the battery pack. The numerical models used to investigate the thermal response of the battery pack under different driving cycle can be divided into two main categories which is electrochemical–thermal model [5,6,9,10] and electro-thermal model [2,11–15].

Electrochemical models and equivalent circuit models are widely used to model the *I–V* characteristics, state of charge (SOC) and thermal response of Li-ion battery. An electrochemical

* Corresponding author. Tel.: +65 65162207; fax: +65 67791459.
E-mail address: mpetayao@nus.edu.sg (L.H. Saw).

http://dx.doi.org/10.1016/j.enconman.2014.07.011
0196-8904/

Nomenclature

C	capacitance, F
C_p	specific heat capacity of the battery, J kg^{-1} K^{-1}
C_Q	cell capacity, A h
E	emissivity
E_m	thermodynamic voltage, V
E_0	battery constant voltage, V
h	convective heat transfer coefficient, W m^{-2} K^{-1}
I_m	current, A
λ	conductive heat transfer coefficient
Q	battery capacity, A h
R	internal resistance, Ω
T	surface temperature of battery, K
T_∞	free stream temperature of air, K
t	time, s
τ_n	time constant n for an R–C branch
V	voltage, V
ρ	density of the battery, kg m^{-3}
σ_{sb}	Stefan–Boltzmann constant, W m^{-2} K^{-4}

Subscript

h	hysteresis
batt	battery
OC	open circuit
avg	average
c	charging
d	discharging

model is used to investigate the electrochemistry reactions in the electrodes and electrolyte at high accuracy, but significant computational resource is required to solve the unknown parameters in partial differential equations [5,10,16–19]. In addition, microscopic information of the battery is also needed such as particle size, current collector and electrode thickness, open circuit voltage of the anode and cathode, and electrolyte conductivity. Unfortunately, these parameters are not provided by the manufacturers and required extensive experimental studies [19]. Hence, electrochemical models are inappropriate to be embedded into the microprocessor in the battery pack management system to provide accurate real time results.

Equivalent circuit model which is a simplification of electrochemical model utilized electrical circuit elements such as voltage sources, resistor and capacitor to represent the *I–V* characteristics of the battery [14,15,20–29]. The equivalent circuit model used Thevenin equivalents, impedances or run time based model to represent the characteristics of the cell [15]. In the Thevenin models, the open circuit voltage is assumed constant and a network of resistors and capacitors is used to track the response of the cell to the transient loads [1,14,15,21,22]. The accuracy of the predictions depends on the number of parallel resistive–capacitive networks. There are numerous resistive–capacitive (RC) network available in the literature such as first order RC [22,23], second order RC [1,24,25] and third order RC [15,26] models. Hysteresis behaviors are often added in the model to improve the prediction. Among these models, most of them are developed based on isothermal conditions and the parameters are constant over a wide range of temperature, limiting their use in on-board battery management system [14,27,28]. On the other hand, impedance based model employed an AC-equivalent impedance model in the frequency domain through impedance spectroscopy. A complex equivalent network (Zac) is utilized to fit the impedance spectra [21]. This type of model cannot predict the response of the cell and is only working for a fixed SOC and temperature setting [29]. The runtime based electrical model used discrete or continuous time implementations in the SPICE simulator to determine the variable in the complex electric circuit network. There are several disadvantages associated with the runtime based electrical model when predicting the current varying load conditions [21]. Among these electrical models, Thevenin model with its reasonable accuracy in predicting the SOC and *I–V* characteristics and temperature is more suitable to be implemented into the vehicle power control system and battery testing.

Hysteresis of open circuit voltage of a battery is a commonly found in Nickel–Metal Hydride (NiMH) and Li-ion cell [30–33]. In Li-ion battery, the hysteresis effect on Lithium Iron Phosphate is more significant than cobalt, nickel or manganese based battery [31–33]. In cobalt, nickel and manganese based Li-ion battery, due to the high gradient in the specific of SOC to open circuit voltage (OCV) relation, the impact of hysteresis on the cell's OCV is negligible. On the other hand, the OCV of the Lithium Iron Phosphate cell shows a plateau voltage over a wide range of SOC. The relationship between OCV and SOC during charging and discharging is path dependent and leads to distortion in OCV to SOC static mapping [33]. The hysteresis will cause unreliable OCV reconstruction in the battery management system that using model-based state estimation approach. However, the hysteresis phenomenon could be reduced by increasing relaxation duration before the OCV of the cell is taken.

In the present work, an equivalent circuit model is used to predict the *I–V* and thermal characteristics of 10 A h Lithium Iron Phosphate pouch cell under constant-current discharge and pulse charge–discharge cycle. The simulation results are validated with the experimental data. The equivalent circuit model is then extended to the whole battery pack to investigate the thermal response of the converted EV battery pack under Urban Dynamometer Driving Schedule (UDDS) and US06 Supplemental Federal Test Procedure (SFTP) test cycles. Through simulations, the electrical and thermal behavior of the cell can be predicted and applied in the EVs power control system and battery thermal management system design.

2. Mathematical models

2.1. Number of RC branches in the equivalent circuit model

Number of RC branches in the equivalent circuit is an important factor determines the accuracy of the prediction and complexity of the model. In this study, the number of RC branches used in the modeling was determined using the transient response of the cell voltage during the relaxation phase when the pulse current was removed. The experimental data are fitted with exponential equations according to the procedures as described in [35,36] and the results are shown in Fig. 1. The *R*-squared value for one RC branch, two RC branches and three RC branches are 0.957, 0.9919 and 0.9963 respectively. From the fitting results, it is shown that one RC branch and two RC branches did not produce a satisfactory match to the experimental data. Although one RC branch and two RC branches are simple, it could not reproduce the experimental results with a sufficient accuracy. Thus, three RC branches with the highest *R*-squared value were selected for this study as a compromise between the accuracy and the complexity.

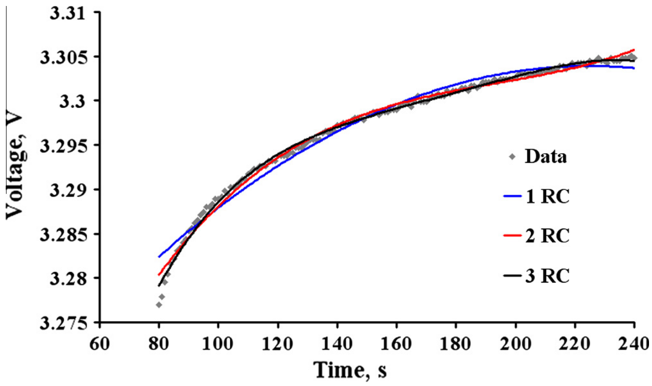

Fig. 1. Curve fit to determine the number of RC branches used in this study.

2.2. Equivalent circuit model

The equivalent circuit model is commonly used to define the electrical and thermal performance of the specific battery in term of current and SOC. In this study, the third order RC model is used to express the electrical behavior of the Lithium Iron Phosphate cell. Parasitic losses are not modeled in the current study due to high coulombic efficiency and relatively low self-discharge as compared to other types of battery [34,35]. The proposed equivalent circuit model includes the temperature effect as an independent variable in the lookup tables to overcome the limitation of the models in the current literature. 5 °C, 25 °C and 40 °C are used as dependent parameters for the resistor, capacitor and open circuit potential. Fig. 2 displays a schematic diagram of the model with one serial resistance and three RC branches. OCV of the RC model can be computed by using Eq. (1) while SOC of the cell is represented by Eq. (2). In total, there are eight parameters in the function of operating conditions used for the study as in Eqs. (1)–(3) [15,36]. The parameters of the battery model are represented by lookup tables. Hysteresis effect was taken into consideration in the model.

$$V_{batt} = V_{oc}(\mathrm{SOC},T) - I_m R_0(\mathrm{SOC},T) + I_m R_t(\tau_1,\tau_2,\tau_3) \tag{1}$$

$$\mathrm{SOC}(t) = \mathrm{SOC}(0) + \frac{1}{C_Q}\int_0^t I_m(t)\cdot dt \tag{2}$$

$$\begin{aligned} R_t = {} & R_1(\mathrm{SOC},T)e^{-\frac{1}{R_1(\mathrm{SOC},T)C_1(\mathrm{SOC},T)}t} + R_2(\mathrm{SOC},T)e^{-\frac{1}{R_2(\mathrm{SOC},T)C_2(\mathrm{SOC},T)}t} \\ & + R_3(\mathrm{SOC},T)e^{-\frac{1}{R_3(\mathrm{SOC},T)C_3(\mathrm{SOC},T)}t} \end{aligned} \tag{3}$$

2.3. Thermal model

Temperature plays an important role in determining the SOC, model parameters and capacity of the cell. Resistance to external convection from battery surface is higher than conduction within the battery [37]. Heat generated by the cell is dissipated through convection and radiation. A general energy balance equation as in Eq. (4) proposed by Bernardi et al. was used to model the total heat generated in the cell [38]. Joule heat and reversible heat are the two main heat sources in the cell. The reversible heat term is computed using the relation of dU/dT with the SOC proposed by Forgez et al. [39].

$$Q_{gen} = i\left(E_0 - V_{batt} + T\frac{dU}{dT}\right) \tag{4}$$

The general energy balance of the battery thermal model is given by Eq. (5) and boundary condition on the outer surface of the cell is defined by Eq. (6). The density, emissivity and thermal conductivity of the pouch cell are given in Table 1.

$$\rho C_p \frac{dT}{dt} = \lambda \frac{\partial^2 T}{\partial x^2} + Q_{gen} \tag{5}$$

$$-\lambda \frac{\partial T}{\partial x}\bigg|_{x=L} = h(T - T_\infty) + E\sigma_{sb}\left(T^4 - T_\infty^4\right) \tag{6}$$

2.4. Thermal model for EV battery pack

Modeling of EV is based on Hyundai Trajet specifications and the battery pack is designed using pouch cell to provide similar power capacity as in the previous study as shown in Table 2 [13]. The battery pack comprised twenty-eight modules and each module is constructed using twenty-four pieces of pouch cell. Since the modules in the battery pack are identical, it is sufficient to study the thermal response of a single module. The thermal response of the battery pack is investigated using the UDDS and US06 driving cycle as shown in Fig. 3.

2.5. Experimental setup and parameter extraction

Commercial 10 A h pouch cells with graphite anode coated on the copper current collector and Lithium Iron Phosphate cathode coated on the aluminum current collector were used in the experiments. The details of the cell are shown in Table 1. The cells were tested at three different temperatures of 5 °C, 25 °C and 40 °C in the environmental chamber (Weiss, WKL 34) to extract the parameters needed. The charging and discharging of the cell was conducted using a battery cycler (Maccor Instrument 4000). Pulse

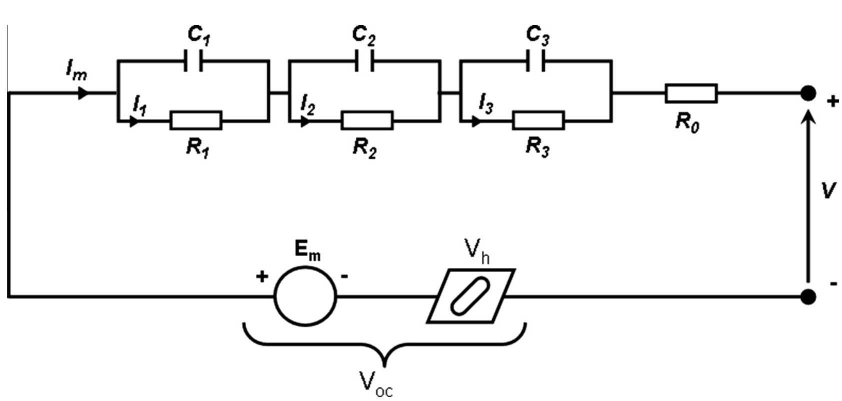

Fig. 2. The equivalent circuit model used for this study.

Table 1
Parameters of the pouch cell.

Parameter	Value	Parameter	Value
Nominal voltage (V)	3.0	Cell thickness (m)	0.0106
Nominal capacity (A h)	10.0	Cell width (m)	0.07335
Weight (kg)	0.261	Cell height (m)	0.1634
Cathode material	$LiFePO_4$	Anode material	Graphite
Specific heat capacity (J kg^{-1} K^{-1})	1200	Aluminum casing thickness (m)	113×10^{-6}
Heat transfer coefficient (W m^{-2} K^{-1}) (estimated)	10	Reference temperature, T_{ref} (K)	298.15
Density (kg m^{-3})	2054.39	Emissivity (estimated)	0.090
Thermal conductivity in y and z direction (W m^{-1} K^{-1}) [40]	18.4	Thermal conductivity in the x direction (W m^{-1} K^{-1})	0.34

Table 2
Vehicle and cooling system specific parameters for the pouch cell.

Parameter	Value
Vehicle mass (kg)	1828
Frontal area (m^2)	3.238
Coefficient of drag (Cd)	0.35
Electric motor	75 kW, 200 Nm max
Battery pack	19.5 kW h
Number of cell per module	24
Number of module	28
Spacing between cell (m)	0.005
A_{ms} per module (m^2)	0.0290
Surrounding temperature (°C)	25

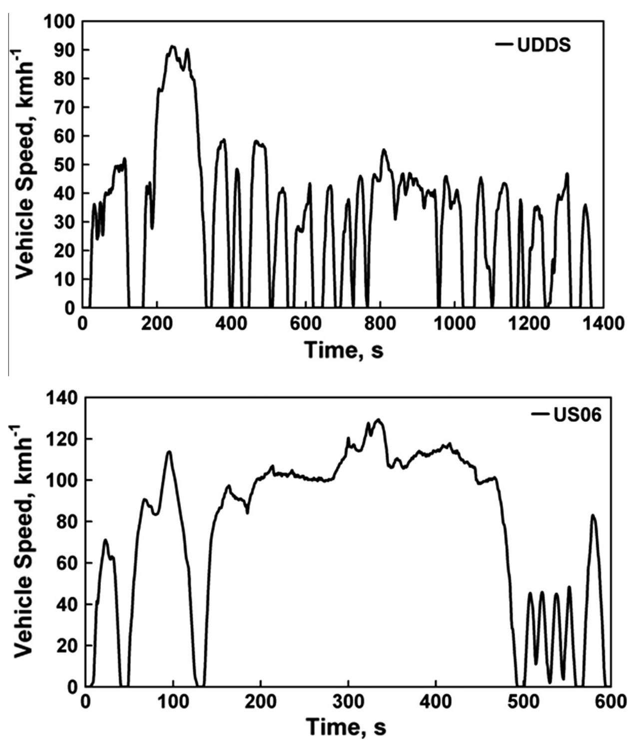

Fig. 3. UDDS and US06 test cycle for the converted EV battery pack.

discharge characterization tests in 10% decrements of SOC at 1 I_t-rate were carried out on 10 A h cells at three different temperatures. One hour rest is imposed between pulse discharges to ensure that the OCV of the cell is stable to obtain a reliable estimation of the model parameters. The temperature of the cell was measured using fourteen thermocouples (T-type) attached to different locations of the cells. A heat flux sensor (Captec) is appended to the center of the cell to measure the heat dissipated from the cell. The measurement of battery surface temperature discharge at different I_t-rates was done at room temperature of 25 °C under natural convection. The temperature readings were recorded using HP 34970A data acquisition system. The specific heat capacity and heat generated in the cell is measured using adiabatic accelerating rate calorimeter (THT ARC). Pulse discharging-charging test at 5 I_t-rate is used as a verification test for the battery model. The bulk cross plane thermal conductivity of the pouch cell was measured using TPS 2500 S (TechMax Technical Co. Ltd.).

2.6. Numerical procedures

The equivalent circuit model parameters for each temperature are calculated using a parameter estimation function in the Matlab-Simulink 2011b. In the resulting model, it is assumed that the pouch cell impedance does not change with the magnitude of discharge current [34]. The pulse discharge profile was iteratively simulated and compared with the experimental results to extract the battery parameters as explained in [34]. The results of the estimated voltage and experimental data at 5 °C, 25 °C and 40 °C are shown in Fig. 4 and the results of the model parameters are shown in Fig. 5.

The parameters of the model circuit elements are described using lookup tables with seven different points of SOC spaced slightly bias toward initial and end of discharge. The parameter values in the two dimensional table are linearly interpolated during simulation to determine the electrical characteristics of the cell. The model is then coupled with the thermal model to estimate the heat generated and surface temperature of the cell under natural convection.

Besides, an independent set of experiment is needed to validate the battery model. The battery model was validated using constant current discharge and pulse discharge and charge. Finally, the validated model is utilized to investigate the thermal response of the battery pack for a converted EV using Hyundai Trajet using UDDS and US06 test cycles under natural convection.

In order to investigate the development of the pouch cell internal temperature under 5 I_t-rate of constant current discharge, the thermal model of the pouch cell as shown in Fig. 6 is used. The pouch cell consists of several layers of electrodes and separator stacking together. In this study, the active material region is assumed to be a single domain with uniform heat generated. The thermal conductivity of the active material region is considered anisotropic. The thermal conductivity in the x direction is 0.34 W m^{-1} K^{-1}, y and z direction are 18.4 W m^{-1} K^{-1}. The heat transfer coefficient of 10 W m^{-2} K^{-1} (natural convection) and 100 W m^{-2} K^{-1} (forced air convection) were used for the current study. The thermal model together with the appropriate boundary conditions was solved with commercial finite element solver, COSMOL Multiphysics 4.3 b. The effects of external current tabs were neglected in this study. Tetrahedral element was used to mesh the pouch cell geometry and direct solver GMRES was chosen with a relative convergence tolerance of 10^{-6} for the modeling. The number of elements used in this study is 1,381,320. All computations were carried out on a computer with a 3.40 GHz Quad core

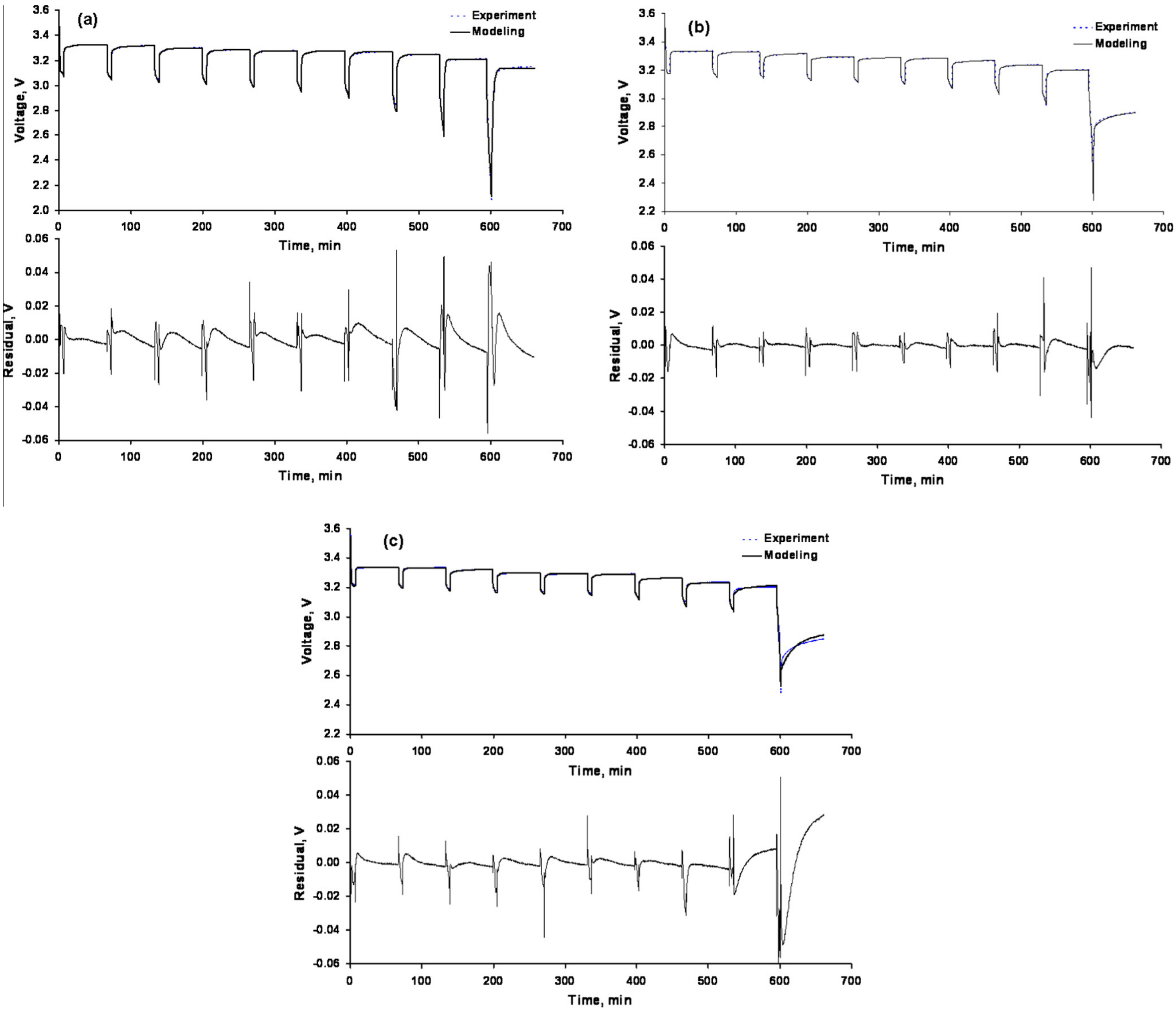

Fig. 4. Experimental and simulated discharge curves and corresponded residual for the pouch cell at the end of estimation process for different temperature: (a) 5 °C, (b) 25 °C and (c) 40 °C.

processor and 32 GB Random Access Memory (RAM). In addition, the grid independent test was carried out to refine the grid size until the simulation results are not affected by further refinement of the mesh.

3. Results and discussion

3.1. Model parameters extraction

Parameter estimation results of the pouch cell at 5 °C, 25 °C and 40 °C are presented in Fig. 4. The comparison of the estimated results and experimental data shown that battery model give a good estimation of the electrical behavior of the cell. The model results are represented by the solid line while experimental results are represented by the dash line. The residuals of voltage error are in millivolts and shown in the lower part of the figure. As shown in Fig. 4, the battery model is able to capture the change of OCV during the discharge process. Toward the end of the discharge process with SOC 10% (last pulse) the residual of the OCV is slightly higher. The maximum residual is about −55 mV, 45 mV and −58 mV for 5 °C, 25 °C and 40 °C respectively. Although the residual of the voltage during pulse discharge is higher at the end of discharge, it would not affect the results of prediction. In the EVs application, the Li-ion battery is normally discharged till 90% of SOC and the cell is not fully discharged to protect the cell. In the battery model, the two dimensional parameters as in Fig. 5 are interpolated over the temperatures to simulate the charging and discharge process of the cell.

As a common practice, the important model parameter, OCV, is measured after a relaxation period following a short and gradual charging or discharging period [32]. In this study, the relaxation duration was varied from 1 min, 30 min to 1 h to investigate the effect of relaxation time on the accuracy of OCV measurement. From the results as shown in Fig. 7(a), there is a large gap between the result by 1 min and 30 min of relaxation, showing that 1 min of relaxation duration is insufficient for accurate OCV measurement. On the other hand, OCV measurement at 30 min is close to OCV reading at 1 h, suggesting that 30 min of relaxation duration is adequate for accurate OCV measurement. Therefore, 1 h relaxation duration was taken in our tests is to ensure the accuracy of measured OCV.

From the results of OCV measured with 1 h of relaxation duration, a discrepancy was found between the OCV measured during

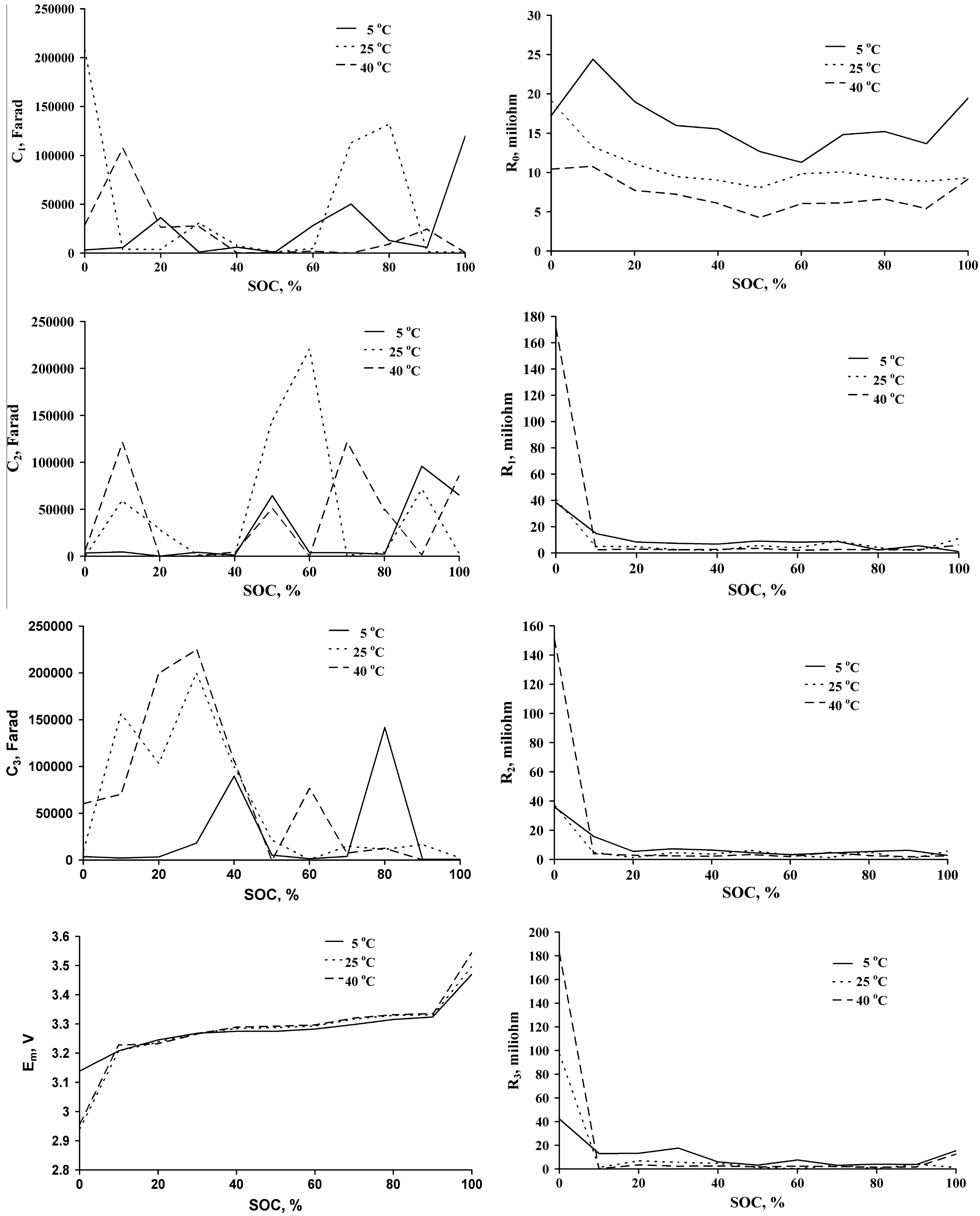

Fig. 5. Model parameters obtained through parameter estimation for the present study.

charging and discharging. This discrepancy existed even when much longer relaxation time was given and this was named as hysteresis phenomenon. Fig. 7(b) demonstrates the hysteresis effect of Lithium Iron Phosphate battery. A common compromise to the hysteresis gap is to adopt the average value of E_m of the OCV as shared OCV in charging and discharging, by doing so, the accuracy in predicting the electrical and thermal behavior would be reduced. In this study, the hysteresis voltage (V_h) as in Eqs. (7)

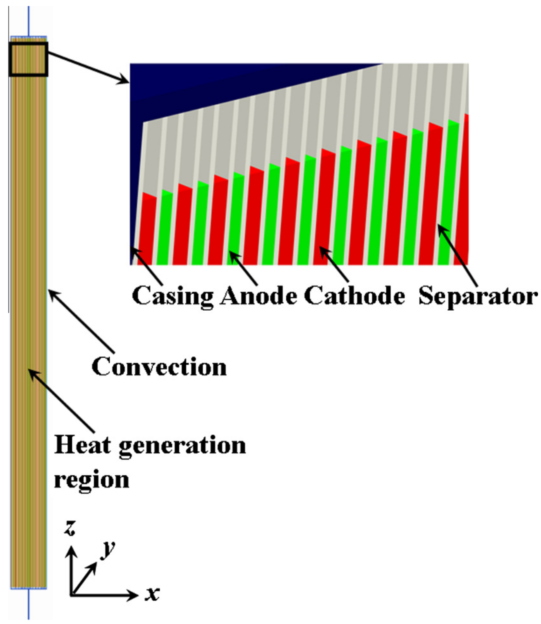

Fig. 6. Schematic of lithium iron phosphate pouch cell thermal model.

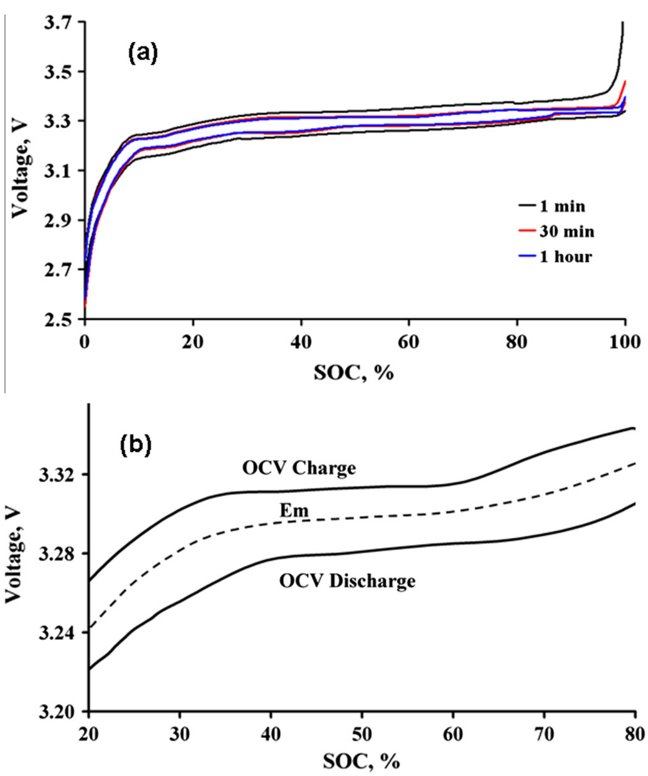

Fig. 7. Typical hysteresis effect of the Lithium Iron Phosphate cell. (a) 1 I_t-rate of charge and discharge with different resting duration. (b) The hysteresis effect of the cell after 1 h of relaxation from 20% to 80% of SOC.

and (8) was adopted to compensate the effect of using E_m and to improve the accuracy of prediction.

$$V_{oc\_charging} = E_m + V_{h\_charging} \tag{7}$$

$$V_{oc\_discharging} = E_m - V_{h\_discharging} \tag{8}$$

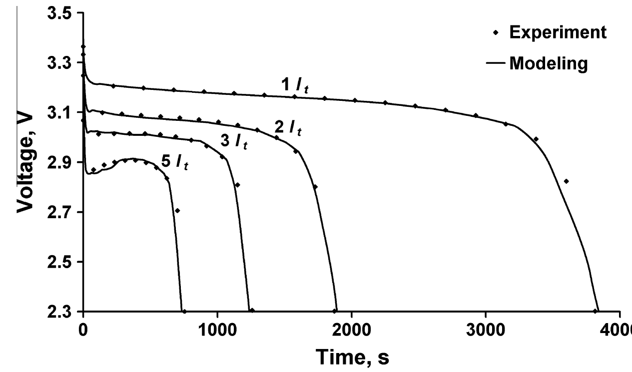

Fig. 8. Voltage prediction results of 1–3 I_t constant current discharge test.

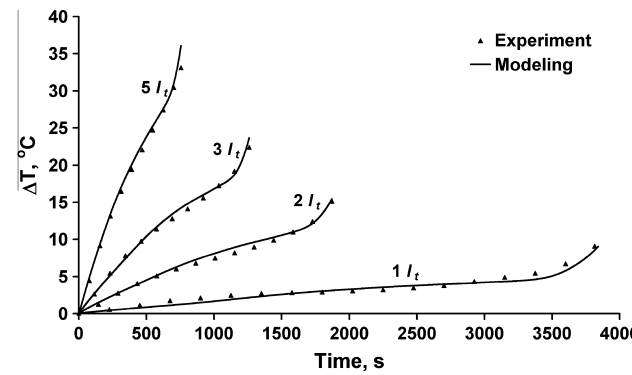

Fig. 9. Temperature rise of the cell at different I_t-rates of discharge.

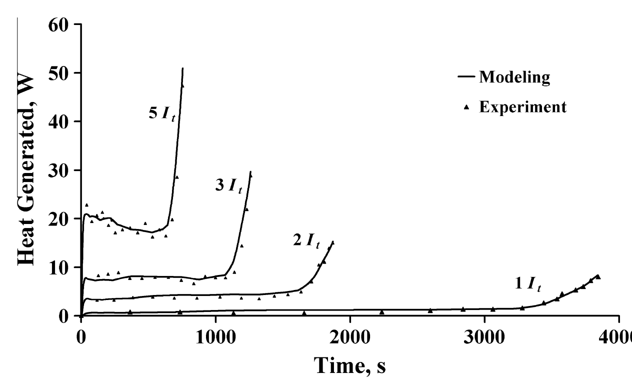

Fig. 10. Comparison between simulation results and experimental data of the pouch cell heat generated at different constant current discharge rates.

3.2. Steady state validation

Experimental validations of electrical and thermal behavior of the battery model under different I_t-rate of discharge are shown in Figs. 8 and 9. The battery model exhibits a good accuracy in predicting the electrical behavior of the cell under steady state condition. The average squared error of the cell voltage for 1, 2, 3 and 5 I_t-rates are 0.0000586, 0.0000203, 0.000387 and 0.000752 respectively.

Comparisons of simulated and measured surface temperature of the pouch cell showed that the battery model produced a good estimation of the thermal behavior of the cell at various I_t-rates under natural convection. The average squared errors of the cell surface temperature for 1, 2, 3 and 5 I_t-rates are 0.0341, 0.0369, 0.0228 and 0.0176 respectively. The maximum surface tempera-

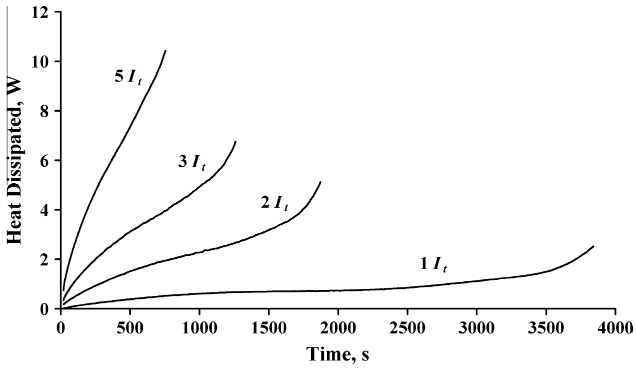

Fig. 11. Heat dissipated from the cell through natural convection at different I_t-rates of constant current discharge.

ture of the cell at 5 I_t-rates is about 61 °C and exceeds the optimum operating temperature limit of the cell. Hence, proper cooling system is recommended for high I_t-rates of discharging or charging to reduce the thermal aging of the cell.

Comparisons of simulated and measured heat generated in the pouch cell at various I_t-rates of discharge are depicted in Fig. 10. Heat generated from the cell is positively correlated to discharge current and capacity of the cell. Average heat generated in the cell at 1, 2, 3 and 5 I_t-rates are about 1.51 W, 4.79 W, 9.02 W and 20.5 W respectively. Modeling results of the heat generated agreed well with the experimental data obtained from the accelerating rate calorimeter. Some deviation of the experimental data with simulation results is noted at 50% of SOC. The effect is also evident in the temperature graph as in Fig. 9. Slightly lower temperatures were measured on the cell surface as compared to simulation results.

Measurement of heat dissipated from the cell using a heat flux sensor is shown in Fig. 11. Maximum heat dissipated from the cell for 1, 2, 3 and 5 I_t rates at the end of the discharging process is 2.58 W, 5.25 W, 6.91 W and 10.58 W respectively. As shown in Figs. 10 and 11, natural convection is effective to dissipate about 30% of the heat generated from the cell and most of the heat generated is kept inside the cell. Average heat dissipation by natural convection to heat generated of the cell is reduced from 58% for 1 I_t-rates of constant current discharge to 29% at 5 I_t-rates of constant current discharge. Hence, at high current discharging process, forced convection is desirable to dissipate the intensive heat generated and prolong the calendar life of the cell.

Fig. 12 shows the internal temperature distribution of the pouch cell at the end of 5 I_t-rate of constant current discharge for $h = 10\ \mathrm{W\ m^{-2}\ K^{-1}}$ (natural convection) and $100\ \mathrm{W\ m^{-2}\ K^{-1}}$ (forced air convection). The maximum internal temperature region of the pouch cell is located at the center of the cell. About 2.7 °C of temperature difference between the center of the cell and the battery surface was found when the heat transfer coefficient is $10\ \mathrm{W\ m^{-2}\ K^{-1}}$ is applied on the battery surface as shown in Fig. 12(a). On the other hand, about 6.3 °C of temperature difference between the center of the cell and the battery surface when the heat transfer coefficient is $100\ \mathrm{W\ m^{-2}\ K^{-1}}$ as shown in Fig. 12(b). As compared to the excellent thermal conductivity of aluminum casing, the active material of the cell is a poor thermal conductor. Although the current collectors of the cell are made of copper and aluminum, porous electrodes and separator which are poor thermal conductivity, preventing the heat generated from the cell being effectively dissipated to the outer

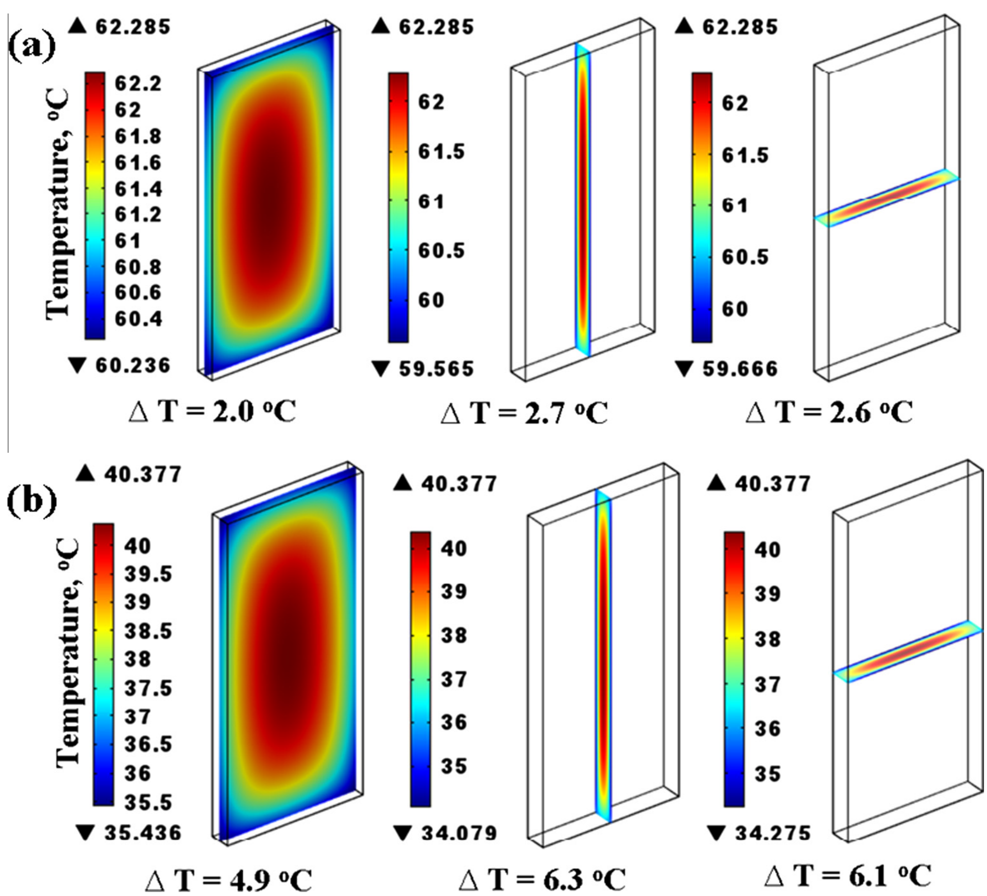

Fig. 12. Predicted variation of internal temperature of the pouch cell at the end of 5 I_t-rate of discharge: (a) $h = 10\ \mathrm{W\ m^{-2}\ K^{-1}}$ and (b) $h = 100\ \mathrm{W\ m^{-2}\ K^{-1}}$.

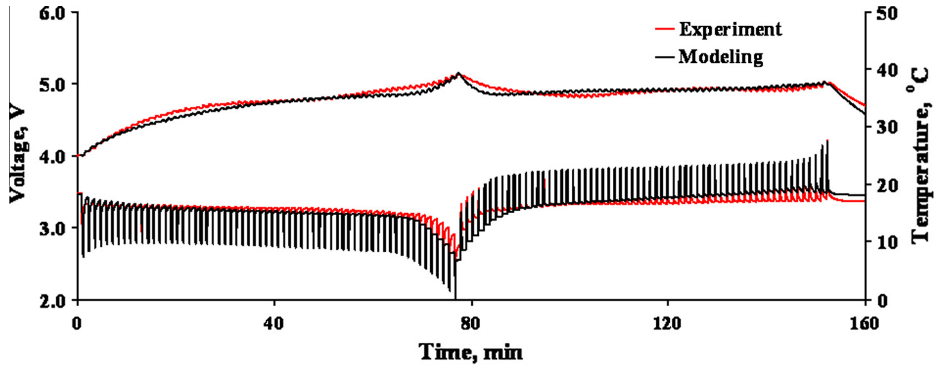

Fig. 13. Comparison between simulation results and experimental data for 5 I_t-rate of pulse discharging and charging for the pouch cell.

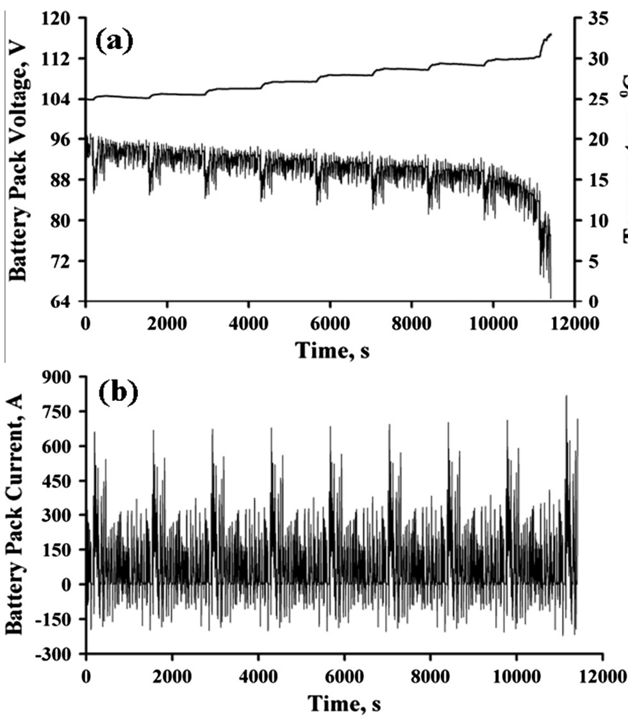

Fig. 14. Electrical and thermal responses of the battery pack to the UDDS test at 25 °C under natural convection.

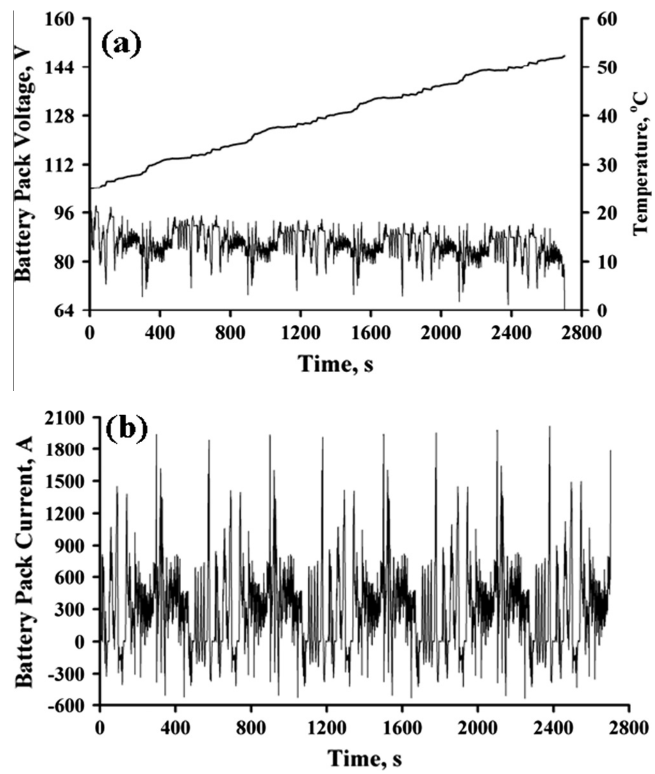

Fig. 15. Electrical and thermal responses of the battery pack to the US06 test at 25 °C under natural convection.

environment. Hence, the safety of the battery cannot be ensured by examining the surface temperature. Compared to cylindrical cell, pouch cell with a large flat surface is more favorable for thermal management. In addition, enhancing the thermal conductivity of the active material region inside the cell is more effective to improve the heat dissipation of cell [41].

3.3. Dynamic behavior validation

In order to further validate the battery, 5 I_t-rate of pulse charging-discharging were performed on the pouch cell. The simulation results against the experimental data are presented in Fig. 13. The simulation results agreed well with the experimental data, except during the end of discharging and charging process. The cause of the discrepancy is explained by the slightest deviation in the estimation of the model parameters at the end of discharging. The proposed battery model regenerated voltage response of the cell with the average squared error of 0.00212. Besides, the accuracy of the thermal model is satisfactory. Average squared error of 0.000435 was reached. The close agreement of the simulation results with experimental data on the Lithium Iron Phosphate pouch cell indicates that the proposed battery model gives an accurate prediction of the electrical and thermal behavior of the Lithium Iron Phosphate cell in the steady state as well as the dynamic state.

3.4. Electrical and thermal response of the battery pack

To ensure the battery model performs well in the real life application, UDDS and US06 test was served as a reference to investigate the thermal response of the battery pack. The overall duration of UDDS test is 1369 s with peak velocity of 91 km h^{-1} while overall duration of US06 test is 600 s with peak velocity of 129 km h^{-1}. As shown in Figs. 14 and 15, the battery pack is able to complete 8.3 cycles of UDDS test and 4.5 cycles of US06 test before reaching the cutoff voltage of 64.4 V. The maximum current withdrawn from the battery pack is 818 A during the end of the cycle. On

the other hand, the charging current into the battery pack during regenerative braking is 217 A as shown in Fig. 14(b). As shown in Fig. 14(a), the temperature of the battery pack increased constantly during the cycle and reached the maximum at the end of the cycle. The average temperature of the cell at the end of the UDDS test is about 33 °C under natural convection and the cells temperature is within the optimum operating temperature limit of the Li-ion battery. Average 5.2 kJ of heat is generated by a single cell in the battery pack during the UDDS test cycle. Throughout the UDDS cycle, 88.81 MJ of energy is utilized to propel the vehicle for targeted speed while 9.85 MJ of energy is recovered through regenerative braking. On the other hand, the average temperature of the cell at the end of US06 test could reach 52.3 °C. As shown in Fig. 15(b), the maximum current withdrawn from the battery pack is 2003 A during the acceleration to pick up the desired velocity. On the other hand, the charging current into the battery pack during regenerative braking is 538 A which is about 2 I_t-rate of pulse charging. The simulation results predict that more heat is generated on an aggressive US06 driving cycle as compared to less aggressive UDDS test cycle and average 11.5 kJ of heat is generated per cell throughout the test. About 75.53 MJ of energy is used to drive the vehicle while 7.4 MJ of energy is recovered through regenerative braking. Therefore, an active battery thermal management system is needed for the EVs that operated in aggressive driving conditions to remove the excessive heat generated from the cells and prevent the heated cells from thermal runaway. Besides, the battery thermal management system also helps to prolong the cycle life of the cell by ensuring the cells operated at optimum temperature range and maintain the temperature uniformity of the cells in the battery pack.

4. Conclusions

The proposed battery model is capable of modeling the electrical and thermal behavior of Lithium Iron Phosphate cell under different operating conditions with good accuracy. The battery model was validated using a constant current discharge and 5 I_t-rate of pulse current charge and discharge. The results of modeling showed a good agreement with experimental results of voltage and temperature over a wide range of temperature and SOC of the pouch cell. Lithium Iron Phosphate cell shows a more noticeable hysteresis phenomenon as compared cobalt, manganese and nickel cathode system. However, the effect of hysteresis can be minimized by prolonging the resting duration before OCV of the cell is taken. The heat generated from the cell is positively correlated with the I_t-rates. Natural convection is capable to dissipate only 30% of the heat generated from the cell and most of the heat is kept inside the cell. This is explained by the poor thermal conductivity of active material. Therefore, using active cooling or improving the thermal conductivity of the electrodes, electrolyte, filler and decreasing the thickness of the separator can effectively dissipate the heat generated and reduce the thermal aging of the cell. Lastly, the validated battery model was used to investigate the thermal behavior of EV battery pack under UDDS and US06 test. At the end of the cycle, the average surface temperature of the cell could reach 36 °C. Although the average surface temperature of the cell is well below the ideal operating temperature range of the cell (40 °C), a well designed active thermal management system is desired for the EV battery pack to prolong the cycle life of the cell and ensure the safety and reliable operation of the battery pack.

Acknowledgement

This work was supported by a Grant No. EPD090005RFP(A) from Energy Market Authority Singapore.

References

[1] Jung S, Kang D. Multi-dimensional modeling of large-scale lithium-ion batteries. J Power Sources 2014;248:498–509.
[2] Pesaran AA. Battery thermal models for hybrid vehicle simulations. J Power Sources 2002;110:377–82.
[3] Saw LH, Tay AAO. Thermal modeling and management of Li-ion batteries for electric vehicles. In: Proceedings of the ASME 2013 international technical conference and exhibition on packaging and integration of electronic and phonic microsystems; 2013.
[4] Karditsas N. 2012 DOE vehicle technologies program review. In: Annual merit review and peer evaluation meeting. <http://www1.eere.energy.gov/vehiclesandfuels/pdfs/merit_review_2012/energy_storage/es138_karditsas_2012_p.pdf> [retrieved October 2013].
[5] Smith K, Wang CY. Power and thermal characterization of a lithium-ion battery pack for hybrid electric vehicles. J Power Sources 2006;160:662–73.
[6] Gu WB, Wang CY, Liaw BY. The use of computer simulation in the evaluation of electric vehicle batteries. J Power Sources 1998;75:151–61.
[7] Zolot M, Pesaran AA, Mihalic M. Thermal evaluation of Toyota Prius battery pack. In: The future car congress; 2002.
[8] Pesaran AA, Swan D, Olson J, Guerin JT, Burch S, Rehn R, et al. Thermal analysis and performance of a battery pack for a hybrid electric vehicle. In: 15th Electric vehicle symposium; 1998.
[9] Bizeray A, Duncan SR, Howey DA. Advanced battery management system using fast electrochemical modeling. In: 4th IET hybrid and electric vehicles conference HEVC; 2013.
[10] Smith KA, Rahn CD, Wang CY. Control oriented 1D electrochemical model of lithium ion battery. Energy Convers Manage 2007;48:2565–78.
[11] Chen Y, Evans JW. Three-dimensional thermal modeling of lithium-polymer batteries under galvanostatic discharge and dynamic power profile. J Electrochem Soc 1994;141:2947–55.
[12] Awarke A, Jaeger M, Pischinger S. Comparison of model predictions with temperature data sensed on-board from the Li-ion polymer cells of an electric vehicle. SAE Int 2012. http://dx.doi.org/10.4271/2011-01-2443.
[13] Saw LH, Somasundaram K, Ye Y, Tay AAO. Electro-thermal analysis of lithium Iron phosphate battery for electric vehicles. J Power Sources 2014;249:231–8.
[14] Hu X, Li S, Peng H. A comparative study of equivalent circuit models for Li-ion batteries. J Power Sources 2012;198:359–67.
[15] Kroeze RC, Krein PT. Electrical battery model for use in dynamic electric vehicle simulations. In: Proceedings of the 2008 IEEE power electronics specialists conference; 2008. p. 1336–42.
[16] Doyle M, Newman J. Comparison of modeling predictions with experimental data from plastic lithium ion cells. J Electrochem Soc 1996;143:1890–903.
[17] Prade E, Di Domenico D, Creff Y, Bernard J, Sauvant-Moynot V, Huet F. Simplified electrochemical and thermal model of $LiFePO_4$–graphite Li-ion batteries for fast charge applications. J Electrochem Soc 2012;159:A1508–19.
[18] Saw LH, Ye Y, Tay AAO. Electrochemical–thermal analysis of 18,650 lithium iron phosphate cell. J Energy Convers Manage 2013;75:162–74.
[19] Dennis DW, Battaglia VS, Belanger A. Electrochemical modeling of lithium polymer batteries. J Power Sources 2002;110:310–20.
[20] He H, Xiong R, Guo H, Li S. Comparison study on the battery models used for energy management of batteries in electric vehicles. Energy Convers Manage 2012;64:113–21.
[21] Chen M, Rincon-Mora GA. Accurate electrical battery model capable of predicting runtime and I–V performance. IEEE Trans Energy Convers 2006;21:504–11.
[22] Tsang KM, Sun L, Chan WL. Identification and modeling of lithium ion battery. Energy Convers Manage 2010;51:2857–62.
[23] Chiang YH, Sean WY, Ke JC. Online estimation of internal resistance and open circuit voltage of lithium-ion batteries in electric vehicles. J Power Sources 2011;196:3921–32.
[24] Benger R, Wenzl H, Beck HP, Jiang M, Ohms D, Schaedlich G. Electrochemical and thermal modeling of lithium-ion cells for use in HEV or EV application. J World Electr Veh 2008;3.
[25] Dubarry M, Liaw BY. Development of a universal modeling tool for rechargeable lithium batteries. J Power Sources 2007;174:856–60.
[26] Andre D, Meiler M, Steiner K, Wimmer Ch, Soczka-Guth T, Sauer DU. Characterization of high-power lithium-ion batteries by electrochemical impedance spectroscopy. I. Experimental investigation. J Power Sources 2011;196:5334–41.
[27] Hu Y, Yurkovich S, Guezennec Y, Yurkovich BJ. A technique for dynamic battery model identification in automotive applications using linear parameter varying structures. Control Eng Pract 2009;17:1190–201.
[28] Rahmoun A, Biechl H, Rosin A. Evaluation of equivalent circuit diagrams and transfer functions for modeling of lithium-ion batteries. J Electr Control Commun Eng 2013;2:34–9.
[29] Buller S, Thele M, Doncker RWD, Karden E. Impedance based simulation models of supercapacitors and Li-ion batteries for power electronic applications. IEEE Trans Ind Appl 2005;41:742–7.
[30] Thele M, Bohlen O, Sauer DU, Karden E. Development of a voltage-behavior model for NiMH batteries using an impedance-based modeling concept. J Power Sources 2008;175:635–43.
[31] Barker J, Pynenburg R, Koksbang R, Saidi MY. An electrochemical investigation into the lithium insertion properties of Li_xCoO_2. Electrochem Acta 1996;41:2481–8.

[32] Roscher MA, Bohlen O, Vetter J. OCV hysteresis in Li-ion batteries including two-phase transition materials. Int J Electrochem 2011. http://dx.doi.org/10.4061/2011/984320.
[33] Tang X, Mao X, Lin J, Koch B. Li-ion battery parameter estimation for state of charge. In: Proceedings of the 2011 American control conference; 2011. p. 941–6.
[34] Huria T, Ceraolo M, Gazzarri J, Jackey R. High fidelity electrical model with thermal dependence for characterization and simulation of high power lithium battery cells. In: Proceedings of the 2012 IEEE international electric vehicle conference; 2012. http://dx.doi.org/10.1109/IEVC.2012.6183271.
[35] Ceraolo M, Lutzemberger G, Huria T. Experimentally-determined models for high-power lithium batteries. In: Proceedings of the SAE 2011 world congress & exhibition; 2011. http://dx.doi.org/10.4271/2011-01-1365.
[36] Huria T, Ludovici G, Lutzemberger G. State of charge estimation of high power lithium iron phosphate cells. J Power Sources 2014;249:92–102.
[37] Rao L, Newman J. Heat-generation rate and general energy balance for insertion battery systems. J Electrochem Soc 1997;144:2697–704.
[38] Bernardi D, Pawlikowski E, Newman J. A general energy-balance for battery systems. J Electrochem Soc 1985;132:5–12.
[39] Forgez C, Do DV, Friedrich G, Morcrette M, Delacourt C. Thermal modeling of a cylindrical $LiFePO_4$/graphite lithium-ion battery. J Power Sources 2010;195:2961–8.
[40] Ye Y, Saw LH, Shi Y, Somasundaram K, Tay AAO. Effect of thermal contact resistances on fast charging of large format lithium ion batteries. J Electrochim Acta 2014. http://dx.doi.org/10.1016/j.electacta.2014.04.134.
[41] Chen SC, Wang YY, Wan CC. Thermal analysis of spirally wound lithium batteries. J Electrochem Soc 2006;153:A637–48.